

Analysis of Activity Dependent Development of Topographic Maps in Neural Field Theory with Short Time Scale Dependent Plasticity

Nicholas Gale^{1*}, Jennifer Rodger², Michael Small², Stephen Eglén¹

¹ *Centre for Mathematical Sciences, Wilberforce Rd, Cambridge CB3 0WA*

² *School of Biological Sciences, 35 Stirling Hwy, Crawley WA 6009, Australia*

³ *School of Physics, Mathematics, and Computer Science, 35 Stirling Hwy, Crawley WA 6009, Australia*

Abstract

Topographic maps are a brain structure connecting pre-synaptic and post-synaptic brain regions. Hebbian-based plasticity mechanisms working in conjunction with spontaneous patterns of neural activity generated in the pre-synaptic regions play a critical role in appropriate topographic development. Studies performed in mouse have shown that these spontaneous patterns can exhibit complex spatial-temporal structures which existing models cannot incorporate. Neural field theories are appropriate modelling paradigms for topographic systems due to the dense nature of the connections between regions and can be augmented with a plasticity rule general enough to capture complex time-varying structures.

We propose a theoretical framework for studying the development of topography in the context of complex spatial-temporal activity fed-forward from the pre-synaptic to post-synaptic regions. Analysis of the model leads to an analytic solution corroborating the conclusion that activity can drive the refinement of topographic projections. The analysis also suggests that biological noise is used in the development of topography to stabilise the dynamics. MCMC simulations are used to analyse and understand the differences in topographic refinement between wild-type and the $\beta 2$ knock-out mutant in mice. The time scale of the synaptic plasticity window is estimated as 0.56 seconds in this context with a model fit of $R^2 = 0.81$.

Key Words Topographic maps, neural field theory, STDP, plasticity, spontaneous activity, Hebbian dynamics, neural organisation.

arXiv:2107.13272v3 [q-bio.NC] 24 Jan 2022

1 Introduction

A topographic map is a ubiquitous brain structure which connects two brain regions: a pre-synaptic region and post-synaptic region [1]. The structure is defined by the relationship that cells that are physically neighbouring in the pre-synaptic region will connect to physically neighbouring cells in the post-synaptic region and is the simplest instance of a topological map [2]. Topographic maps have been shown to have remarkable regeneration and re-organisational properties but this study will focus only on their development [3, 4, 5, 6]. Historically, topographic development was thought to be mediated by either Hebbian activity-based mechanisms, or chemotactic signalling mechanisms but these now are thought to more typically work in tandem [7].

The dense feed-forward connectivity pattern present in topographic systems make neural field theories (NFT) an attractive paradigm for modelling electrical activity patterns in topographic systems. An NFT is a continuum model where the spiking activity of many neural inputs are averaged into a smoothly varying function over temporal and spatial locations. A theory of topographic development was proposed for an NFT which relied on static inputs in the pre-synaptic region resulting in activity patterns in the post-synaptic region stabilising to be time-independent and thus allowing a simple Hebbian plasticity rule to be applied [8]. The requirement for activity to stabilise before updating weight is also a feature of more general cortical map plasticity models [9, 10]. A more recent study used an NFT to model topography in the somatosensory cortex under thalamocortical plasticity using Oja’s rule [11]. The assumption of static inputs limits the range of biological systems for which the theory developed in these works can apply in development.

A proposed candidate model organism is the mouse retinotopic map: the set of connections that map retinal cells in the eye to cells in the superior colliculus (SC) [12, 13]. This is distinct from other topographic projections such as somatosensory and tonotopic maps [14]. The mouse develops topography using three mechanisms: chemotaxis, competition, and activity based refinement [15, 7]. The activity component of development involves three stages of spontaneously generated retinal waves which are thought to refine a coarse topography of dendritic arbours (grown from afferent neurons which are guided topographically by a combination of chemotaxis and competitive interactions) down into a precise point-to-point mapping [7, 16, 17]. Disruptions to the patterning of these waves have been explored by knocking out

the nicotinic-acetylcholine receptor $\beta 2$ which generates fast-spreading waves and thus a hyper-correlation – where neurons are correlated at a far greater inter-neuron distance than in wild type – between any two given retinal cells [18]. The effect of the $\beta 2$ knock-out is to reduce the precision of the resulting topographic map: the receptive field of a given SC location is large with respect to wild-type [19, 15, 20].

Modelling efforts in this field have focused recently on predicting map structure of various mutants and a unified model of chemotaxis, activity, competitive mechanisms was shown to give the best account of the data [21, 22, 23, 24]. The mutants examined were predominantly genetic perturbations of the chemical gradients and therefore activity was not considered as a major focus. These models by construction are unable to capture the various spatio-temporal statistics of the retinal waves condensing them all into a single correlation measure as a function of SC-distance; a corollary is that they have not been able to reproduce the effect of the $\beta 2$ knock-out when the correlation function is adjusted to match the knock-out [25]. While historical models have allowed for the incorporation of spatial patterning in the input stimulus, they do not consider time variations in stimulus at a time-scale below that of plasticity implicitly assuming all transient neuronal information (such as spatio-temporally patterned stimulus waves) is averaged out [26, 27, 9]. Recent efforts in a separate unified model which can incorporate dynamic activity were not able to quantitatively account for the $\beta 2$ mutant data and are too computationally demanding for rigorous statistical analysis [28]. There is a need for theory which can analyse and predict the effects of time-varying stimuli on the organisational structure of maps.

In this paper we aim to develop theory for modelling the development of topographic systems which can incorporate complex spatial-temporal patterns of activity, such as those seen in mouse. A candidate theoretical framework of Hebbian-based plasticity that can incorporate time-signatures of activity, spike timing dependent plasticity (STDP), has been developed for NFT [29, 30]. The framework is continuous, rather than discrete, which allows us to investigate synaptic efficacy between locations rather than modelling individual synapses. We shall demonstrate that NFT can support the refinement and establishment of precise topography via waves of propagating activity and biologically reasonable Hebbian learning rules and therefore establish it as a useful model to study the development of topographic systems. Moreover, we will validate the model against the $\beta 2$ knock-out and make predictions about the time-scale on which the Hebbian

Symbol	Description
S	Feed-forward kernel: pre-to-post regions
W	Recurrent kernel: post-to-post region
H	Synaptic evolution by spike-time envelope
Q	Map of membrane potential to spike-rate
u/U	Post-synaptic membrane potential/rates
a/A	Pre-synaptic membrane potential/rates
h	Form of activity waves
Θ	Heaviside Theta function
δ	Dirac-Delta distribution
η	Representation of white noise

Table 1: Symbols which are used to represent biological objects and/or processes. The parameters which are used to specify each functional form are omitted and detailed in later sections.

activity operates. A glossary of symbols that will be used throughout the paper is shown in Table 1.

2 Model

We will choose a simple model architecture that closely imitates the systems of interest: input from a continuous pre-synaptic field of nerve cells stimulates activity in a continuous post-synaptic field of nerve cells via a collection of feed-forward connections. These feed-forward connections will evolve under a plasticity rule governed by the spatio-temporal relations between the input and induced activity in the pre-synaptic and post-synaptic fields respectively. The activity in the post-synaptic field will be supported by inhibitory and excitatory sets of isotropic recurrent (or lateral) connections which, for simplicity, we shall assume to be static; for a description of non-isotropic recurrent kernels refer to [31, 32]. Changes in the feed-forward connections are dictated by firing activity in the pre-synaptic and post-synaptic fields. The activity dynamics in the post-synaptic field will be modelled by a neural field equation which couples a membrane potential and firing activity spatio-temporally. The pre-synaptic field activity could be modelled the same way but because there is no feed-back from the post-synaptic field it is sufficient to simply instantiate it which can be motivated by experimental spiking data [33]. The model architecture is summarised in Figure 1 and we shall now explicitly lay out the details of the model.

Representation of Topography We need to establish what we mean by topography in the continuous sense. We aim to preserve two things: the neighbourhood projection, and the excitatory feed-forward

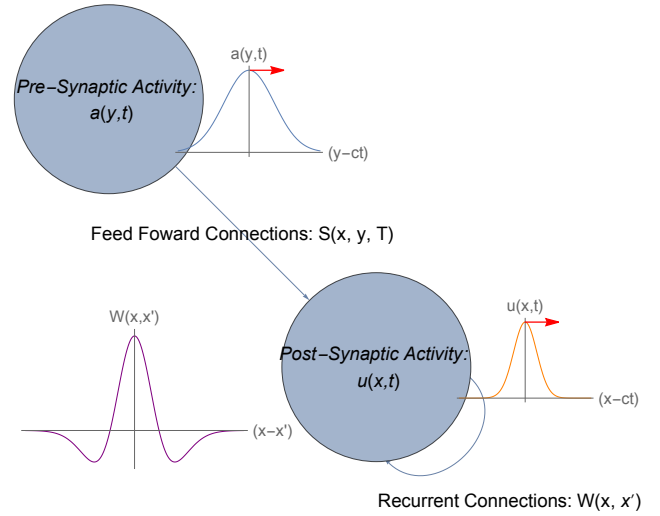


Figure 1: The connections and directionality of the model: activity is fed-forward from the pre-synaptic region by the structure of interest and is spatial-temporally propagated by a time-differential operator and spatial convolution of inhibitory and excitatory recurrent connections. We show cartoons of typical propagating activity patterns and recurrent connections but not feed-forward connections as determining these are the object of this study. The generated signal in the post-synaptic region and the driving signal in the pre-synaptic region are then convolved with a plasticity window to inform the synaptic changes on a slow time scale which is indicated by the variable $T = \epsilon t$ for some small ϵ .

nature of the network. To preserve the neighbour-neighbour relation the connections, here referred to as a synaptic distribution, labelled S , and measured in synapses per mm^2 , should take the form:

$$S(x, y, T) = S(|x - p(y) - \rho|, T), \quad (1)$$

where $p(y)$ is some monotonically increasing function and ρ is some constant to indicate that a coordinate shift still permits a topographic mapping. The excitatory feed-forward nature means that a patch of activation in the pre-synaptic field should activate a local patch of the post-synaptic field associated with its topographically projected location. Therefore, S should decay quickly at infinity, be positive at the topographically projected location, and have a finite (small) radius at which it transitions to being negative. Alternatively, it can be strictly positive but quickly decaying such that it never over-powers the recurrent inhibitory connections; see Figure 2.

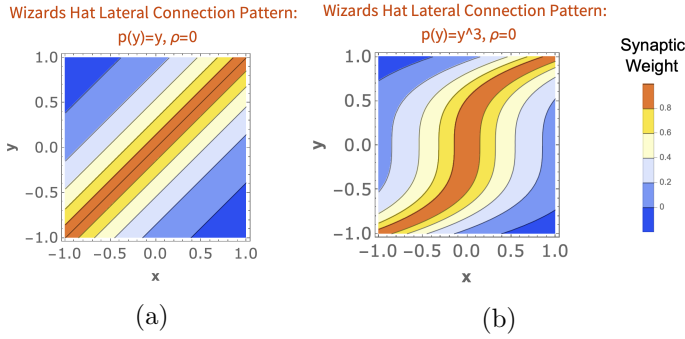


Figure 2: Two examples of topographic organisation using a Wizard hat style function: a) shows a linear relationship between axes and for while b) shows a cubic relationship between axes. Both are topographic but a) has an even representation of the pre-synaptic field across the post-synaptic field while b) compresses the representation at the boundary and enlarges the interior.

Neural Field Theory We shall choose the NFT formulation proposed by Amari (1970) which considers both excitatory and inhibitory connections in the same kernel W [8]. We shall consider a kernel S that also couples the pre-synaptic and post-synaptic regions. It is this kernel in which we aim to demonstrate the evolution of topography. We shall denote the electrical activity, measured in millivolts (mV), of the pre-synaptic field by $a(x, t)$ and in the post-synaptic field by $u(x, t)$, and choose the firing rate function to be a sigmoid-logistic function:

$$Q(u) = \frac{Q_{\max}}{1 + \exp(-\beta(u - \theta))}, \quad (2)$$

where β and θ dictate the steepness of the curve and the threshold respectively, and Q_{\max} is the maximal firing rate; the units of each are mV^{-1} , mV , and spikes per second and can be found in Table 2. The activity dynamics are then governed by the internal dynamics mediated by W and the input provided through the pre-synaptic field, $Q(a)$, and its transfer through S :

$$\begin{aligned} u(x, t) + \tau \frac{\partial u(x, t)}{\partial t} - \int_{-\infty}^{\infty} W(x, x') Q(u(x', t)) dx' \\ = \int_{-\infty}^{\infty} S(x, y, T) Q(a(y, t)) dy. \end{aligned} \quad (3)$$

Note that the time variable T is on a much slower time scale which is realised by setting $t = \epsilon T$ for $0 < \epsilon \ll 1$. For the purposes of solving equation 3 these connections can be considered effectively constant. We assume for simplicity that the recurrent connections W remain constant throughout the course of synaptic development and are homogenous. Following Robinson

(2011) a plasticity window is defined as a rapidly decaying envelope H that weights the cross-correlation of the input and response signals in a population in the same fashion as biologically-inspired plasticity rules weight individual spikes of a neuron [29]. These plasticity windows have been observed in several organisms and brain regions; a typical window has a time constant on the order of 10s of milliseconds but have been observed to be on the order of 10s of minutes [34, 35, 36, 37, 38]. The average synaptic dynamics are given by averaging over a time-window which is longer than the time-scale of the plasticity window and of the inverse frequencies of the forcing and the response stimuli but shorter than any long term plasticity changes:

$$\tau' \frac{dS(x, y, T)}{dT} = \int_{-\infty}^{\infty} \langle U(x, T + s) H(s) A(y, s) \rangle ds, \quad (4)$$

where $U = Q(u)$, $A = Q(a)$ (the firing rates of the post-synaptic and pre-synaptic populations respectively), $\langle \cdot \rangle$ denotes averaging, and τ' is the time-scale of synaptic dynamics. In the case of no electrical activity present in the pre-synaptic field there will be a constant level of spontaneous firing A inducing an electrical activity and firing rate U which in turn will lead to run-away synaptic dynamics. We are interested in the dynamics of the average rate of synaptic change and the expected synaptic values; in later sections this will be taken as an adiabatic expansion and averaging over stimulus input locations. Therefore, the above equation should include a noise term η , which we shall take to have a strength κ , to incorporate the small deviations of spontaneous activity:

$$\begin{aligned} \tau' \frac{dS(x, y, T)}{dT} = \int_{-\infty}^{\infty} \langle U(x, T + s) H(s) A(y, s) \rangle ds \\ + \kappa \eta(x, y, t). \end{aligned} \quad (6)$$

Regularisation Several regularisation rules have been posed to stabilise these unstable Hebbian dynamics and are broadly classified in the form of subtractive and multiplicative rules [30]. In this study we choose a subtractive normalisation rule to stabilise the dynamics, assuming there is some atrophic factor to regulate the unbounded growth of synapses, governed by parameter λ , released at each location:

$$\begin{aligned} \tau' \frac{dS(x, y, T)}{dT} + \lambda S(x, y, T) = \\ \int_{-\infty}^{\infty} \langle U(x, T + s) H(s) A(y, s) \rangle ds + \kappa \eta(x, y, t). \end{aligned} \quad (7)$$

The idea of a synaptic decay on the basis of metabolic demands has also been introduced in a study of or-

ganisational behaviour in V1 [39]. We shall study the dynamics of equation 7 for the remainder of this text.

Perturbations We shall assume that in the absence of forcing activity that the post-synaptic field relaxes to a constant solution i.e. there is a constant level of spontaneous firing in the pre-synaptic and post-synaptic fields; note that this is not necessarily the case [40]. We then assume that all activity dynamics are small perturbations from these constant rates. Furthermore, if one makes the assumption that the firing rates can be expressed as perturbations from a baseline firing rate, $U(x, t) = U_0 + \delta U(x, t)$ and $A(x, t) = A_0 + \delta A(x, t)$, then taking Fourier transforms the average change in plasticity in the un-regularised dynamics can be expressed as:

$$\frac{1}{2\pi} \int_{-\infty}^{\infty} \delta \hat{U}(x, \omega) \hat{H}(\omega)^* \delta \hat{A}(y, \omega)^* d\omega, \quad (8)$$

where $\hat{\cdot}$ denotes the Fourier transform, and \cdot^* denotes complex conjugation [29].

Input Stimulus We shall consider two classes of input stimulus: mono-directional and bi-directional (radial) waves. Mono-directional waves propagate either to the left/right at speed c starting at some time t_0 and some starting position y_0 finally finishing at some time t_1 . We note that these terms are rooted in a two dimensional consideration of the problem. A mono-directional wave might travel along a single radial angle whilst a radial wave travels isotropically. These choices allow for a description of the waves observed in the retina [33, 18, 41]. Of the two the mono-directional wave is the most appropriate model but the bidirectional wave is an equivalent but analytically preferable case as we show in Section 3. Letting $r(y, t) = y - ct - y_0$, these inputs accordingly take the form:

$$a(y, t) = (\Theta(t - t_0) - \Theta(t - t_1))h(r(y, t)). \quad (9)$$

Radial inputs are similar, simply propagating in both directions:

$$a(y, t) = \frac{(\Theta(t - t_0) - \Theta(t - t_1))(h(r(y, t)) + h(r(y, -t)))}{2}. \quad (10)$$

In both cases h is used to denote the shape of the propagating wave-form. The choice of h is left to be general but can be thought of as a travelling Gaussian wave-packet. A function may be approximated by a linear sum of appropriately weighted Gaussian's and so this forms a basis set and we will consider the simple case in Section 3.1.

Plasticity Windows There are two general forms of plasticity considered: time symmetric and time asymmetric plasticity. Time symmetric plasticity, also called Correlation Dependent Plasticity (CDP), means that connections are strengthened by spikes that are separated by short times and weakened by medium-long time separated spikes, but in which the ordering of the spikes is not important. Time asymmetric plasticity, or STDP, means that not only does the temporal closeness of pre-synaptic and post-synaptic spikes matter but the ordering in which they occur: post-synaptic firing that occurs before pre-synaptic firing weakens the connection and vice-versa. A canonical form of these two rules expressed as a plasticity envelope is given by:

$$H(s) = \begin{cases} A_+ \exp(-\frac{s}{t_p}) & s \geq 0 \\ A_- \exp(\frac{s}{t_p}) & s < 0 \end{cases} \quad (11)$$

where $A_- = A_+$ for CDP and $-A_- = A_+$ for STDP, and t_p is the time-scale of the plasticity [30]. The Fourier transforms of these learning rules are:

$$\hat{H}_{CDP}(\omega) = \frac{2A_+}{1 + \omega^2 t_p^2} \quad (12)$$

$$\hat{H}_{STDP}(\omega) = \frac{2A_+ \omega i t_p}{1 + \omega^2 t_p^2} \quad (13)$$

In summary, a membrane signal is generated in the post-synaptic region on a fast-time scale which is supported by recurrent connections and generated by input from a pre-synaptic region. The spatial-temporal patterns of the pre-synaptic and post-synaptic activity then inform synaptic changes between the two regions on a slow time scale in accordance with a plasticity rule.

3 Analysis

We shall make the assumption that our connectivity kernels, pre-synaptic stimuli, and post-synaptic activity and firing rates are elements of Schwartz space i.e. the functions and derivatives that define these rates decay quickly at long range and they are localised. This assumption is made to ensure bio-physical realism. Connectivity kernels typically have short-range and long-range interactions but they do not interact at all with very distal connections and their functions must accordingly decay at infinity. Similarly, due to these recurrent connectivity kernels, electrical signals only seem to be able to support themselves on finite distances and they too must accordingly decay. The assumption of Schwartz functions ensures that we can take Fourier transforms and makes formulating our problem in Fourier space desirable.

Approximating Input Stimulus The inputs that we specified earlier are biologically realistic but will become more tractable if we are able to remove one of the Heaviside functions; this would amount to a stimulus propagating to infinity after being initialized. To show this we need to demonstrate that the synaptic change induced by this different stimulus is arbitrarily small when compared to the synaptic change induced by the true stimulus. This is realised by the rapid decay of the plasticity window and shown formally in Lemma 1; see Appendix A.

Activity Dynamics It was reasoned on physical grounds that in the absence of pre-synaptic stimulation the only post-synaptic solution is a static, constant level of activity; we are interested in calculating perturbations away from these baseline levels. We shall assume the baseline is sufficiently close to the origin that the logistic function is analytical and has a convergent Taylor series expanded around $u = u_0$. Therefore, a good approximation is:

$$Q(u) = Q(u_0) + uQ'(u_0). \quad (14)$$

This can then be inserted in equation (3) and a Fourier transform can be taken to yield:

$$\hat{u}(k, \omega) = Q(u_0)\Gamma(k, \omega)(\hat{W}(k) + \hat{S}(k))\delta(k)\delta(\omega) \quad (15)$$

$$+ Q'(u_0)\hat{S}(k)\Gamma(k, \omega)\hat{a}(k, \omega), \quad (16)$$

where $\Gamma(k, \omega) = (1 + i\tau\omega - \hat{W}(k))^{-1}$. Now recognising that $Q(u_0)\Gamma(\omega, k)(\hat{W}(k) + \hat{S}(k))\delta(k)\delta(\omega)$ corresponds to the static solution, i.e. the baseline activity level, we can write an expression for the Fourier transform of the perturbation of the activity level:

$$\delta\hat{U}(k, \omega) = \hat{S}(k)\Gamma(k, \omega)\hat{a}(k, \omega), \quad (17)$$

where $U(x, t) = Q(u(x, t))$. The Fourier Transform of the perturbation from the baseline rate in the pre-synaptic field, $\delta A(y, t)$ is trivial to compute: $\delta\hat{A}(k, \omega) = \delta\hat{a}(k, \omega)$. This is all we need to explicitly compute the synaptic change between any two points in the pre-synaptic and post-synaptic field.

Synaptic Dynamics We shall assume that the synaptic field, and synaptic changes are isotropic; $S(x, y, T) = S(x - y, T)$ for all T . Then making the approximation of the firing rate, and taking spatial Fourier transforms the synaptic change can be written:

$$\begin{aligned} \delta(p+k)\frac{d\hat{S}(k, T)}{dT} &= \delta(p+k)(S_0 - S_1\hat{S}(k, T)) \\ &+ S_2\int_{-\infty}^{\infty}\hat{a}(\omega, p)\hat{a}(\omega, k)^*\hat{H}(\omega)^*\hat{S}(k, T)^*\Gamma(\omega, k)d\omega, \end{aligned} \quad (18)$$

where S_0 , S_1 , and S_2 have absorbed the time constant, regularisation constants, baseline firing rate, and the Fourier normalisation terms. We have kept the sign of S_1 negative to indicate its relationship with the decay constant λ . Integrating with respect to p , the above equation may be solved as:

$$\frac{d\hat{S}(k, T)}{dT} = S_0 - S_1\hat{S}(k, T) + \quad (19)$$

$$S_2\hat{S}(k, T)^*\int_{-\infty}^{\infty}\mathcal{B}(\omega)\hat{a}(\omega, k)\hat{H}(\omega)^*\Gamma(\omega, k)d\omega, \quad (20)$$

where $\mathcal{B}(\omega) = \int_{-\infty}^{\infty}\hat{a}(\omega, p)^*dp$. The connectivity kernel S in position space is physically required to be real. We can write it as the composition of odd and even functions. Then, from conjugate symmetry it follows that its Fourier transform is then composed of a real part consisting of the linear combination of the Fourier transforms of its even components, and an imaginary part consisting of the linear combination of the Fourier transforms of its odd components. For S to remain real its derivative must have an even function as its real component, and an odd function as its imaginary component. Denoting,

$$G(k) = \int_{-\infty}^{\infty}\left(\int_{-\infty}^{\infty}\hat{a}(p, \omega)^*dp\right)\hat{a}(\omega, k)\hat{H}(\omega)^*\Gamma(k, \omega)d\omega, \quad (21)$$

we can see that if $G(k)$ is even and real, or odd and purely imaginary, then the above equation can be separated into odd and even parts and solved as two independent ODEs. Attention will be restricted to the even form of $G(k)$ as we will show in the next section that this must be the case. Denoting $S_O(x, T)$ and $S_E(x, T)$ to be the odd and even parts of the coupling function in position space these ODEs are then:

$$\frac{d\hat{S}_O(k, T)}{dT} = -(S_1 + S_2G(k))\hat{S}_O(k, T) \quad (22)$$

$$\frac{d\hat{S}_E(k, T)}{dT} = S_0 + (S_2G(k) - S_1)\hat{S}_E(k, T). \quad (23)$$

Therefore, in the asymptotic limit, provided $S_1 + S_2G(k) > 0$ the odd components of the initial organisation decay to zero and provided $S_1 > S_2G(k)$ the even components have solution:

$$\hat{S}_E(k) = \frac{S_0}{S_1 - S_2G(k)}. \quad (24)$$

The final organisation is therefore dictated by the initial even components and the form of $G(k)$. We will show that $G(k) > 0$ which is sufficient to satisfy the above conditions. The form of G is prescribed the learning rule employed and the input stimulus used, we shall refer to it as the training function.

Mono-Directional Propagation If we suppose the input stimulus is $a(y, t) = \Theta(t)h(y - ct - y_0)$ then it is fairly straightforward to show that the training function G is not even and therefore will not work, for our purposes, as a training function. However, if we assume that the synaptic changes are adiabatic or reasonably small and we assume that the proportions of waves propagating left and right are equal then the average synaptic dynamics induced by inputs of the mono-directional form (equation 9) are the same as the dynamics induced by inputs of the radial form (equation 10). Therefore, we shall continue the analysis for radially propagating inputs.

Radial Propagation Presume the input stimulus is in the form $a(y, t) = \Theta(t)(h(y - ct - y_0) + h(y + ct - y_0))$. Taking two Fourier transforms yields:

$$\hat{a}(p, \omega) = \frac{1}{2}e^{-2\pi iy_0 p} \hat{h}(p) (\delta(\omega + cp) + \delta(\omega - cp) + \frac{2i\omega}{\pi(\omega - cp)\pi(\omega + cp)}) \quad (25)$$

Then integrating with respect to p by using the Cauchy Residue Theorem and evenness of the last term and \hat{h} gives:

$$\int_{-\infty}^{\infty} \hat{a}(p, \omega)^* dp = \left(1 + \frac{2}{c}\right) \hat{h}\left(\frac{\omega}{c}\right)^* \cosh\left(2\pi iy_0 \frac{\omega}{c}\right). \quad (26)$$

$G(k) = G(k; y_0)$, and if we assume that the synaptic changes at each time step are small then the average synaptic change can be written as:

$$\left\langle \frac{d\hat{S}(k, T)}{dT} \right\rangle = S_0 - S_1 \hat{S}(k, T) + S_2 \hat{S}(k, T) \langle G(k; y_0, c) \rangle. \quad (27)$$

The asymptotic limit, which we are ultimately interested in, will approach this average and for the remainder of this work we shall drop the angle brackets. Let $g(k; c) = (\hat{H}(ck)^* \Gamma(k, ck) + \hat{H}(-ck)^* \Gamma(k, -ck))/c$. Equation (26) can then be inserted into the expression for $G(k)$ and the Dirac-Deltas can be integrated. Then, we integrate out y_0 by assuming it is distributed over some interval of length L giving exponential integral functions which vanish as $y_0 \rightarrow \infty$ yielding:

$$\frac{d\hat{S}(k, T)}{dT} = S_0 + \hat{S}(k, T) \left(S_2 g(k; c) |\hat{h}(k)|^2 - S_1 \right), \quad (28)$$

Showing that $g(k; c)$ is even may be done by direct substitution for both STDP and CDP rules under the assumption that both W and h are even. It then follows that all $G(k)$ are even. It remains to be shown

that $G(k)$ is restricted to being non-negative or non-positive. All the scaling constants are positive and it is therefore clear for the STDP rule that $G(k) \geq 0$, while for the CDP rule $G(k)$ is never non-positive and is only non-negative if $\hat{W}(k) < 1$. It is certainly possible that this is the case, but it is not true for common choices of W . W is typically chosen to be in the form of a ‘‘wizards-hat’’ with short-range excitation and long range inhibition which is theoretically grounded and observed experimentally [42, 43].

3.1 Computational Analysis and Parameter Estimation

So far, we have proceeded in a general manner without much reference to the recurrent connections or input stimulus (with the exception of wave-speed c) and the parameters and functional forms that characterise them. Here we shall specify explicit choices for both of these and examine the consequences on the organisation via computational means. We shall also try and estimate key parameters which contribute to the width, or arbor size, of the final organisation by means of Markov Chain Monte Carlo (MCMC) applied to wild-type and $\beta 2$ knockout data. This estimation allows us to both validate the model and estimate biological quantities which have not yet been experimentally examined.

We choose a Gaussian to describe the wave-form of the input stimulus with amplitude and width (variance) parameters of σ_1 and σ_2 respectively and with Fourier Transform $\hat{h}(k) = \sigma_1 \sigma_2 \exp(-k^2 \sigma_2^2 / 2)$. We then choose a difference of two Gaussians to describe the recurrent connections: $\hat{W}(k) = r_1 \exp(-k^2 r_1^2 / 2) - R_1 r_2 \exp(-k^2 r_2^2)$. The choice ensures that the dimensional requirements for the propagator are satisfied and that $|W(k)| < 1$ for a suitable choice of recurrent connection parameters. These choices mean that there are 16 key biological parameters: $u_0, \tau, \tau', \kappa, \lambda, A_p, t_p, Q_{\max}, \beta, \theta, c, \sigma_1, \sigma_2, R_1, r_1, r_2$.

Parameter Analysis Examination of equation 24 shows that S_0 (or κ/τ') serves to stabilise the dynamics at the cost of introducing noise - the Fourier spectrum of a biologically realistic organisation will decay to a constant i.e. to a baseline level of white noise. A tolerable level of system noise is expected and we will assume that this noise can be filtered by some means. The denominator dictates the deviations from this noise and noting that for both CDP and STDP $G(k) \rightarrow 0$ and $G(k) > 0$ we have that physically viable solutions enforce $0 < G(k) < S_1/S_2$ and non-viable solutions contain pairs of singularities (via evenness of

Param.	Value	Units	Description
u_0	-58	mV	Resting potential
τ	0.1	s	Activity time-scale
τ'	100	s	Synaptic time-scale
κ	0.001	syn.mm ⁻²	Synapse density
λ	0.001	—	Decay rate
A_p	1	syn.mm ⁻² s	Hebbian rate
t_p	1.0	s	Hebbian time-scale
Q_{\max}	1	s ⁻¹	Max firing rate
β	0.26	mV ⁻¹	Rate steepness
θ	-45	mV	Rate threshold
c	0.1	mm s ⁻¹	Wave-speed
σ_1	5	mV	Wave-amplitude
σ_2	0.1	mm	Wave-length
R_1	1.08	mm	Recurrent amplitude
r_1	0.129	mm	Inhibitory length-scale
r_2	0.136	mm	Excitatory length-scale

Table 2: The choices made for each of the biological parameters used throughout the text, unless otherwise stated. The length scale is chosen to reflect the scale at which NFT typically applies in the brain and the appropriate scale for the mouse SC [44]. The resting membrane potential, the threshold voltage, and the voltage scale are estimated to be in line with electrophysiological recordings [45]. These parameters should be carefully measured if a specific biological system is to be closely analysed.

G) where $G(k) > S_1/S_2$ for some k .

We note that an arbitrarily large wave-amplitude σ_1 can force a singularity in both cases and an arbitrarily large c can force a singularity in the STDP case. From this we can deduce for stability in the STDP case that the maximum wave speed is bound by a contour inversely proportional to wave-amplitude and vice-versa. Given the likely biological restrictions on amplitude this implies that wave speed could be dictated in part by wave amplitude. With this in mind we will set $\sigma_1 = 5\text{mV}$ for the remainder of this work. This ensures that there is a baseline distinguishable level of firing when the wave reaches its peak amplitude but the neurons are not near a saturated level thus satisfying the assumptions required for the approximation in equation 14. We see that $u_0, \tau', \lambda, A_p, f_{\max}, \beta, \theta$ are absorbed into S_0, S_1 , and S_2 and their effects on the dynamics are immediate: they dictate the absolute measurable values of the organisation, not the form. We therefore set these parameters according to Table 2 for the remainder of this work.

We can see also that for CDP $G(k)$ attains its global maximum at $k = 0$ meaning that its stability is determined entirely by the relationship between S_1 and S_2 .

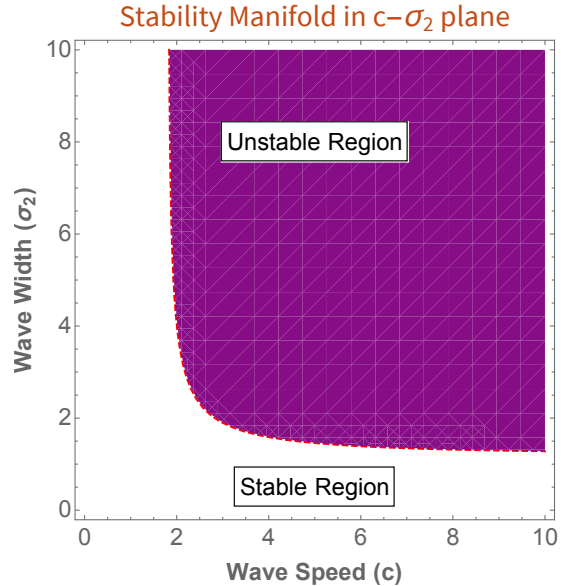


Figure 3: The manifold in (c, σ_2) space which defines the stability of the final organisation. Below the surface solutions do not exhibit singularities and the training function is deemed to be stable; in general, small choices for the parameters exhibit stable synaptic organisations at the cost of arbitrarily small amplitude. The manifold appears to be well-above reasonable estimates for these parameters, ensuring the model is likely stable in plausible biological scenarios.

Furthermore, with CDP synaptic changes have the potential be to large with no parameter available to mitigate them, in the STDP case the small timescale ensures that the changes are small and the adiabatic assumption is satisfied. We proceed only with the STDP case noting that extending the analysis to a CDP rule would be straightforward but care must be taken in the choice of parameters.

These choices, while considered, have reduced the problem to a single learning rule and several key parameters. We stress that the other parameters must be carefully measured for accurate predictions and are in some sense non-trivial: one can manipulate them biologically and cause a bifurcation in the organisation dynamics. Figure 3 demonstrates the manifold in the $c-\sigma_2$ plane for which the model presents plausible (stable) solutions. We have shown only a 2-dimensional slice of the overall manifold for which there are no solutions with singularities, but care should be taken in ensuring that any solution of interest lies within the volume of this manifold for all parameters.

Fourier Space The Fourier transform of S has a characteristic bump near the origin which decays to a constant representing a baseline level of noise i.e.

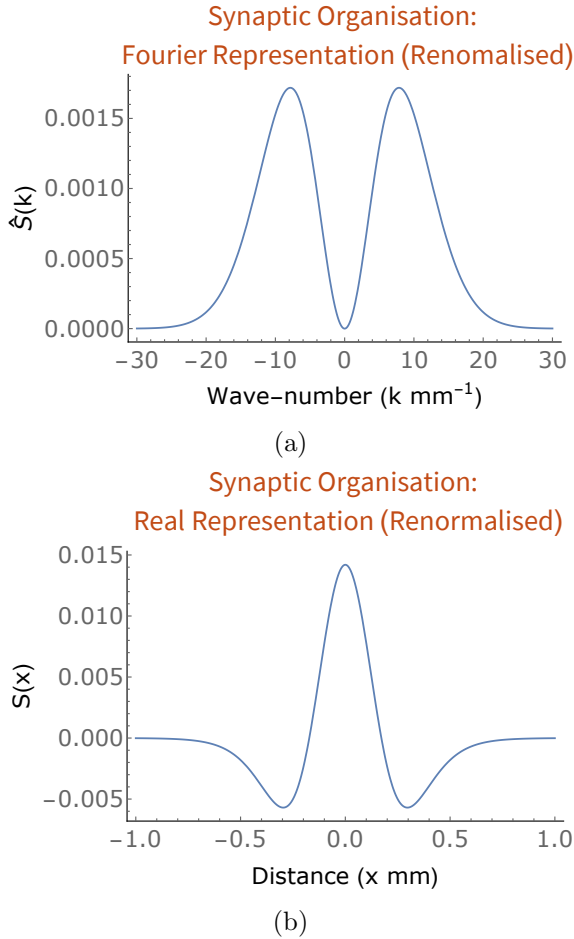


Figure 4: A typical organisation generated with the parameters shown in Table 2 with (a) showing the representation in Fourier space, and (b) the representation in real space after re-normalisation.

$\hat{S}(k) = c_0 + \hat{S}(k)$ where $\hat{S}(k)$ is a symmetric function decaying quickly to zero. Note that it is possible for $\hat{S}(k)$ to fall below the noise level which implies that the system will be out of phase and suppress signals at this wave length. A typical representation in Fourier and real space is shown in Figure 4a.

The distribution of the connections in physical space can be found by inverting its Fourier representation which presents a problem with the inclusion of the Dirac-Delta distribution introduced by c_0 . This problem can be circumvented by realising that the baseline constant representation of all frequencies represents white noise which can be therefore be renormalised and omitted; see Figure 4b. This re-normalisation is done under the assumption that provided the amplitude of $\hat{S}(k)$ provides a high enough signal-to-noise ratio then this system will be absorbed into already present biological noise which is filtered out in downstream calculations.

Refinement The steady state solution of the synaptic distribution S takes its maximum at the origin and rapidly decays at large distances. The distributions feed-forward capability is therefore dictated by the magnitude at the origin and the rate of the decay. For precise signal transmission (or a refined retinotopy) the width of the distribution should be small with respect to the length scale. We can estimate width by taking the inverse of the wave-length that maximises the power spectrum :

$$\Omega(\vec{\rho}) = \frac{1}{\operatorname{argmax}_k |\hat{S}(k; \vec{\rho})|}, \quad (29)$$

where $\vec{\rho}$ represents the vector of parameters which define the model. We shall examine the width relationships in the plane of several pairs of variables within a stable region containing no singularities; shown in Figure 5. Refinement tends to decrease in accordance with decreases in $c, \sigma_2, (r_1/r_2), R_1, t_p,$ and τ . On the biological scales of interest for the current work the decreases do not appear to be substantial in the R_1 and τ directions. In general the relationships between the variables are non-linear.

Sensitivity In the context of refinement it is prudent to consider which parameters affect the models prediction of the width which we have defined. The width given by equation (29) will satisfy $dS(k; \vec{p})/dk = 0$ which inserted into equation (24) yields:

$$\frac{dg(k; \vec{p}_g)}{dk} = 0, \quad (30)$$

where $\vec{p}_g = \{c, \tau, t_p, \sigma_2, R_1, r_1, r_2\}$. The width will only vary in accordance with these parameters which was confirmed by numerical simulation.

MCMC Parameter Estimation The $\beta 2$ knock-out in mouse has the effect of altering the spatio-temporal patterns of spontaneous activity in the retina and SC during development [18]. The mutant mice have substantially wider arborisations than in wild-type establishing the importance of activity in refining the retinotopic projection [46]. Existing models have not been able to predict this wider arborisation when the patterns of activity associated with the knock-out are replicated in the models mechanisms for activity [25].

We estimate the arborisation widths as $0.24 \pm 0.077\text{mm}$ (wild-type) and $0.48 \pm 0.15\text{mm}$ ($\beta 2$) by taking half the square root of the arborisation area reported by [46]. We estimate the wave speeds as $0.13 \pm 0.015\text{mm s}^{-1}$ (wild-type) and $0.17 \pm 0.03\text{mm s}^{-1}$ ($\beta 2$),

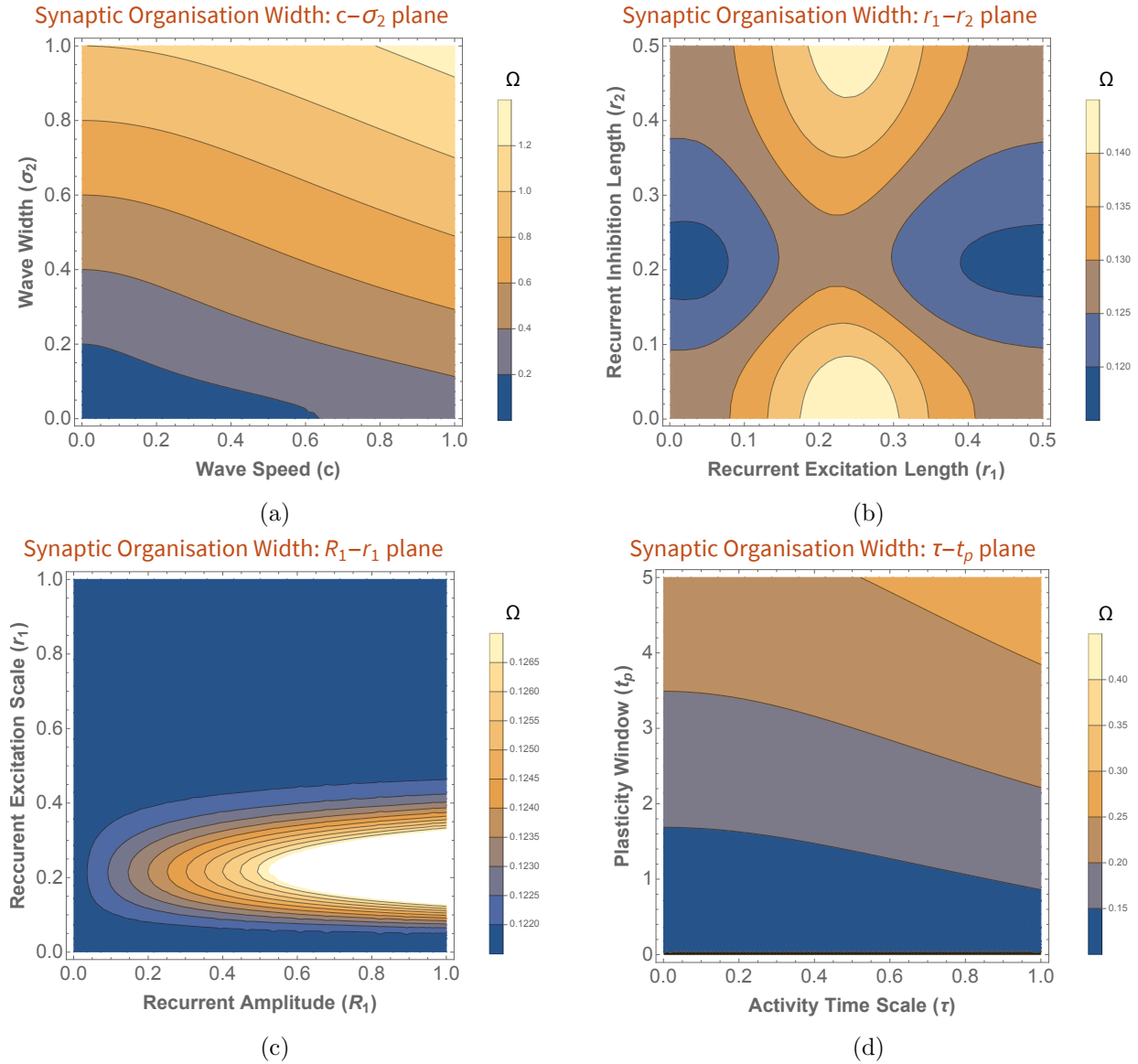


Figure 5: The variation in width (Ω) in four distinct planar slices of the manifold of parameters which influence the models prediction of mean distribution width. Panel (a) shows that width decreases both with wave-speed and wave-width, qualitatively accounting for the differences between the wild-type and $\beta 2$ mutant. Panel (b) shows that width decreases with with the ratio of excitation to inhibition in the recurrent connections W suggesting a smaller zone of excitatory support decreases arbor size. There is an anti-symmetry along the line $r_1 = r_2$ which is expected as the dominant connection type switches along this line. Panel (c) shows that width decreases with recurrent connection amplitude but the effect is not substantial. Panel (d) shows that width predominately decreases in accordance with the plasticity window time-scale, and while the activity time-scale has an effect it is not substantial.

and the wave-widths as $0.11 \pm 0.012\text{mm}$ (wild-type) and $0.20 \pm 0.012\text{mm}$ ($\beta 2$) by taking half the total width reported by Stafford et al 2009 [18]. We estimate the inhibitory and excitatory lengths scales, and amplitude of the recurrent connections to be $0.14 \pm 0.014\text{mm}$ and $0.13 \pm 0.013\text{mm}$, and $1.08 \pm 0.01\text{mm}$ respectively using the data reported by [43]. We take our priors on these parameters to be normal distributions centred on the estimates with standard deviation corresponding to the measurement error. We take uninformative pri-

ors on the time-scale parameters assigning uniform distributions on $[0,1]$ and $[0,10]$ for the activity time scale (τ) and the plasticity window scale (t_p), respectively. The MCMC was completed using a dedicated Mathematica package [47]. The MCMC completed in 10^5 iterations using 6 chains with each parameter initialised within 10% of the mean of its prior. The maximum Gelman-Rubin statistic for convergence was 1.00037 indicating that the chains had converged [48]. The posteriors for each parameter are reported in Figure

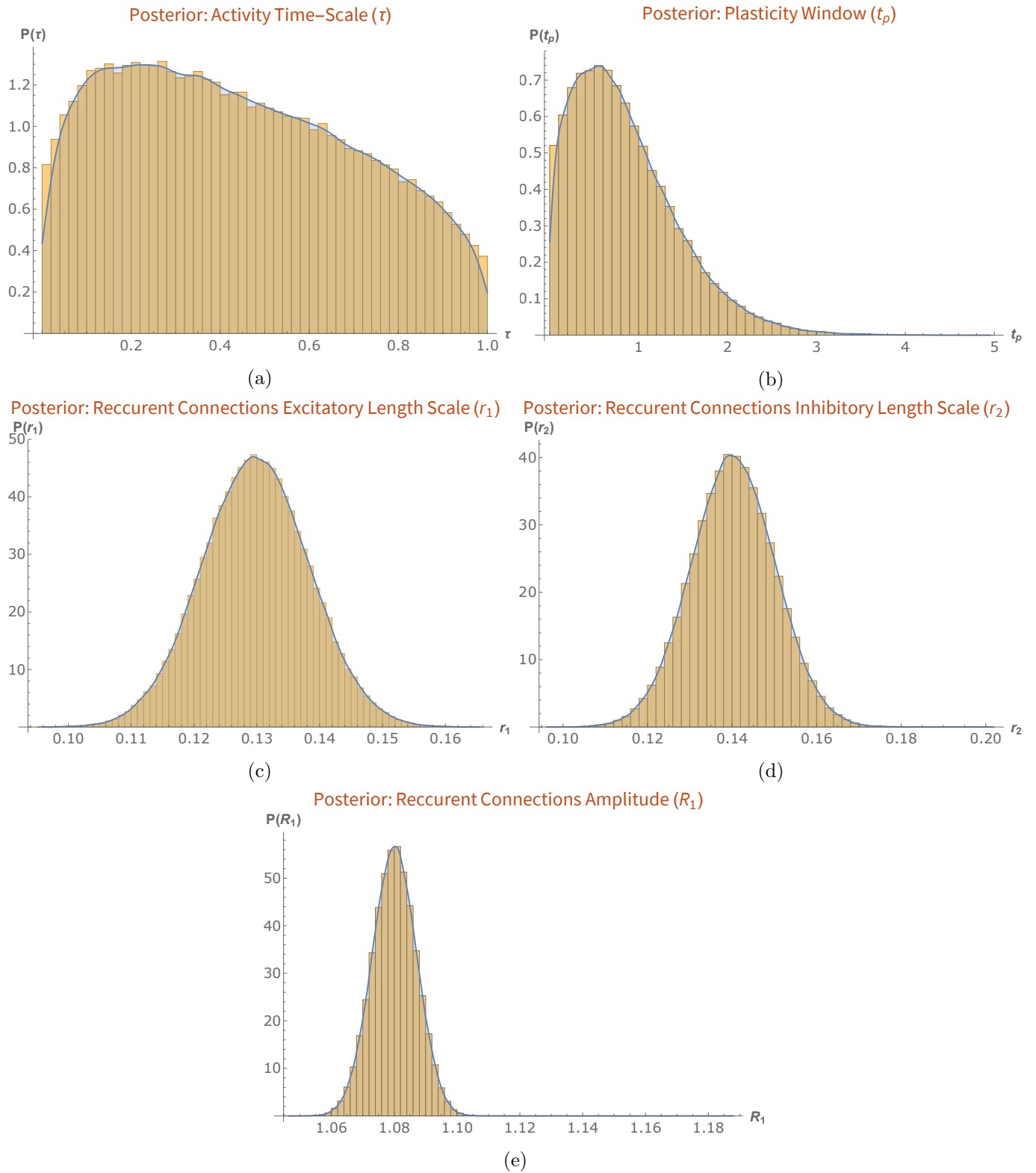


Figure 6: Panel (a) shows the posterior histogram for the time-scale of activity which is broadly distributed through the search space of $[0,1]$ s but biased towards the lower bound. This broad distribution is concordant with the observation that the time-scale of activity induces relatively small variations in the organisation width; see Figure 5. Panel (b) shows the posterior histogram for the time scale of the plasticity window which is maximised around 0.6s. The posterior histograms for the recurrent connection parameters (r_1, r_2, R_1) are shown in Panels (c-e) and are tightly constrained by their informative priors suggesting that there is no predicted effect on these connections in the β_2 mutant. For all histograms presented an empirical distribution curve was fitted and overlain in blue.

6. The posteriors for the recurrent connections parameters, r_1, r_2 , and R_1 remained tightly constrained by their priors, indicating that the prior estimates were well informed and in agreement with the model. The activity time scale is broadly distributed throughout the range $[0,1]$ s with a bias towards 0. The plasticity time-scale is distributed around a maximum of 0.56s. The computed R^2 statistic was 0.81.

4 Discussion

If the model is sound and the biological system is allowed sufficient time to reach a reasonable approximation of the asymptotic state then these results suggest that the computational/synaptic structures developed are primarily a result of activity dynamics. Under this model the chemotactic and competitive mechanisms serve to initialise a coarse isotropic retinotopy from which the activity dynamics can refine and ultimately dictate final synaptic organisation. This interpretation augments the understanding of the establishment of retinotopy by suggesting that the final synaptic organisation can be understood in a large part by understanding the spatio-temporal nature of the input stimulus, the recurrent connectivity, and the learning rule. Should the biological system not employ the learning routine until asymptotic stability then the model will still be able to make predictions about the final organisation given precise enough measurements of the relevant parameters. In both instances the model gives testable hypotheses the former of which has been benchmarked against the mouse wild-type and $\beta 2$ knock-out mutant.

Organisation We have shown that the key aspects of the final organisational structure are dictated by the interplay between the spatio-temporal characteristics of the input stimulus and the structure of the recurrent connections. These dependencies on recurrent connections and input are in accordance with previous analysis performed with a simple Hebbian rule and static input [49]; the model proposed here, however, allows for richer construction in terms of specifying the input and connections by realising full temporal and spatial dynamics, and more complex structure in the final organisation. We have introduced regularisation rules which allow this organisation to take non-trivial structure when supplemented by system noise which we have assumed is able to be renormalised in downstream biological calculations or via some other mechanism. The regularisation necessitates neurotrophic factors being expressed during development. Finally, the measurable aspects of the organisation are dictated

by the precise realisation of the relevant biological parameters.

Refinement The results indicate parameter dependence on wave-speed, wave-width, plasticity time-scales, and the ratio of excitation to inhibition widths in the recurrent connections. Principally, parameter changes that would lead to a tighter correlation structure such as smaller wave-widths, slower wave-speeds, and smaller excitatory zones lead to a smaller width of topographic refinement. Interestingly, the time-scale of the plasticity rule has an effect of the width of the final organisation. The $\beta 2$ knock-out provides a phenomenological test of this component of model. The knock-out exhibits fast-moving, and hyper-correlated, retinal waves which lead to an imprecise topographic mapping - an effect that has not been captured in existing models. Our model suggests that an increase in wave-speed or wave width will lead to a less-refined map reproducing the results of the knock-out *in silico*; see Figure 5.

An MCMC parameter estimation was performed using known errors-in-measurement of wave-speed, wave-width, and organisation width in wild-type and the $\beta 2$ mutant. The model predicts the expected mean width of both wild-type and the $\beta 2$ knock-out within standard error when parametrized by likelihood maximising parameters and provides a good explanation of the variance between the wild-type and mutant ($R^2 = 0.81$). We found the model to be insensitive to the time-scale of activity with the posterior assuming a broad posterior over $[0, 1]$ s with a slight bias towards lower values suggesting that the activity time-scale does not account for much of the variance in organisation width. The posteriors of the parameters of the recurrent connections were largely dictated by their priors suggesting that the priors estimated from available are informative and that the $\beta 2$ knock-out does not have a substantial effect on the recurrent connections, as expected. We do not expect the time-scale of the plasticity window to be affected by the knock-out and thus the MCMC allows us to estimate this parameter on the order of seconds. The timescale of the plasticity window in two closely related biological systems, the *Xenopus* retinotectal projection and rat visual cortex, are estimated to be on the order of 10^{-2} seconds [34, 35]. Plasticity windows can have significantly longer time-scales on the order of 10s of minutes [38]. Our estimate is notably higher than what has been observed in similar systems but is in agreement with the typical duration of a wave of spontaneous activity in the developing retina in mice [50]. We might expect a deviation as we are analysing a different bio-

logical system. This result suggests that the plasticity windows in this system are calibrated to integrate all information contained in a spontaneous wave event.

Future Directions The analysis presented here has made simplifying assumptions about the statistical properties of spontaneously generated waves: these assumptions cannot be expected to hold in general. The analysis was also restricted to one dimension: the two-dimensional case has a much richer topology and is more relevant as the topographic projection is typically organised as a sheet. The analysis can be trivially extended into the plane by using the same assumption: every wave-direction is equiprobable. More realistic wave-statistics can be simulated numerically and examining the properties of the synaptic distribution generated by the data of spontaneous activity in mouse is a future research direction; for example using the model of activity proposed by Godfrey and Eglen (2009) [41, 51, 52].

The model predicts that the time-scale of the plasticity window in developing mouse SC neurons is 1-2 orders of magnitude higher than the scale typically used to describe neuronal plasticity in analogous systems. While we do not claim that this prediction represents a ground truth, the model makes several simplifying assumptions and estimations, it is a good candidate for experimental falsification.

Conclusion We have developed a modelling framework in which the effects of rich spatio-temporal patterns of activity on topographic refinement can be analysed alongside system specific measurements of parameters. The model posits that the final synaptic organisation is dictated in a large part by the characteristics of this activity suggesting a more involved role for activity, spontaneous or otherwise, in the developing visual system. The model explains topographic defects observed in the $\beta 2$ mutant which has had its spontaneous activity patterns altered and on the basis of the mutant and wild-type offers a prediction of the time-scale on which Hebbian refinement operates in mouse development.

Generating Code The code used to perform the analysis and generate the images in this project may be found at https://github.com/Nick-Gale/Neural_Field_Theory_Topographic_Development.

Declaration of Interest: None.

Acknowledgements

We would like to thank Peter Robinson for their comments and discussion on the manuscript.

This research was funded in part by the Wellcome Trust (Grant Reference: 215153/Z/18/Z) and in part by the Australian Postgraduate Award. For the purpose of open access, the author has applied a CC BY public copyright licence to any Author Accepted Manuscript version arising from this submission.

References

- [1] S B Udin and J W Fawcett. Formation of topographic maps. *Annu. Rev. Neurosci.*, 11:289–327, 1988.
- [2] James A Bednar and Stuart P Wilson. Cortical maps. *Neuroscientist*, 22(6):604–617, December 2016.
- [3] D V Buonomano and M M Merzenich. Cortical plasticity: from synapses to maps. *Annu. Rev. Neurosci.*, 21:149–186, 1998.
- [4] M M Merzenich, J H Kaas, J Wall, R J Nelson, M Sur, and D Felleman. Topographic reorganization of somatosensory cortical areas 3b and 1 in adult monkeys following restricted deafferentation. *Neuroscience*, 8(1):33–55, January 1983.
- [5] D Robertson and D R Irvine. Plasticity of frequency organization in auditory cortex of guinea pigs with partial unilateral deafness. *J. Comp. Neurol.*, 282(3):456–471, April 1989.
- [6] J H Kaas, L A Krubitzer, Y M Chino, A L Langston, E H Polley, and N Blair. Reorganization of retinotopic cortical maps in adult mammals after lesions of the retina. *Science*, 248(4952):229–231, April 1990.
- [7] Jianhua Cang and David A Feldheim. Developmental mechanisms of topographic map formation and alignment. *Annu. Rev. Neurosci.*, 36:51–77, July 2013.
- [8] S Amari. Dynamics of pattern formation in lateral-inhibition type neural fields. *Biol. Cybern.*, 27(2):77–87, August 1977.
- [9] Jean-Luc R Stevens, Judith S Law, Ján Antolík, and James A Bednar. Mechanisms for stable, robust, and adaptive development of orientation maps in the primary visual cortex. *J. Neurosci.*, 33(40):15747–15766, October 2013.
- [10] James A Bednar, Amol Kelkar, and Risto Miikkulainen. Scaling self-organizing maps to model large cortical networks. *Neuroinformatics*, 2(3):275–302, 2004.
- [11] Georgios Is Detorakis and Nicolas P Rougier. A neural field model of the somatosensory cortex: formation, maintenance and reorganization of ordered topographic maps. *PLoS One*, 7(7):e40257, July 2012.
- [12] Shinya Ito and David A Feldheim. The mouse superior colliculus: An emerging model for studying circuit formation and function. *Front. Neural Circuits*, 12:10, February 2018.
- [13] Tania A Seabrook, Timothy J Burbridge, Michael C Crair, and Andrew D Huberman. Architecture, function, and assembly of the mouse visual system. *Annu. Rev. Neurosci.*, 40:499–538, July 2017.
- [14] J H Kaas. Topographic maps are fundamental to sensory processing. *Brain Res. Bull.*, 44(2):107–112, 1997.
- [15] Todd McLaughlin, Christine L Torborg, Marla B Feller, and Dennis D M O’Leary. Retinotopic map refinement requires spontaneous retinal waves during a brief critical period of development. *Neuron*, 40(6):1147–1160, December 2003.
- [16] A Bansal, J H Singer, B J Hwang, W Xu, A Beaudet, and M B Feller. Mice lacking specific nicotinic acetylcholine receptor subunits exhibit dramatically altered spontaneous activity patterns and reveal a limited role for retinal waves in forming ON and OFF circuits in the inner retina. *J. Neurosci.*, 20(20):7672–7681, October 2000.
- [17] Alessandro Maccione, Matthias H Hennig, Mauro Gandolfo, Oliver Muthmann, James van Copenhagen, Stephen J Eglén, Luca Berdondini, and Evelyne Sernagor. Following the ontogeny of retinal waves: pan-retinal recordings of population dynamics in the neonatal mouse. *J. Physiol.*, 592(7):1545–1563, April 2014.
- [18] Ben K Stafford, Alexander Sher, Alan M Litke, and David A Feldheim. Spatial-temporal patterns of retinal waves underlying activity-dependent refinement of retinofugal projections. *Neuron*, 64(2):200–212, October 2009.
- [19] Thomas D Mrsic-Flogel, Sonja B Hofer, Claire Creutzfeldt, Isabelle Cloëz-Tayarani, Jean-Pierre Changeux, Tobias Bonhoeffer, and Mark Hübener. Altered map of visual space in the superior colliculus of mice lacking early retinal waves. *J. Neurosci.*, 25(29):6921–6928, July 2005.
- [20] Anand R Chandrasekaran, Daniel T Plas, Ernesto Gonzalez, and Michael C Crair. Evidence for an instructive role of retinal activity in retinotopic map refinement in the superior colliculus of the mouse. *J. Neurosci.*, 25(29):6929–6938, July 2005.

- [21] J J Johannes Hjorth, David C Sterratt, Catherine S Cutts, David J Willshaw, and Stephen J Eglén. Quantitative assessment of computational models for retinotopic map formation. *Dev. Neurobiol.*, 75(6):641–666, June 2015.
- [22] Jason W Triplett, Cory Pfeiffenberger, Jena Yamada, Ben K Stafford, Neal T Sweeney, Alan M Litke, Alexander Sher, Alexei A Koulakov, and David A Feldheim. Competition is a driving force in topographic mapping. *Proc. Natl. Acad. Sci. U. S. A.*, 108(47):19060–19065, November 2011.
- [23] Ruben A Tikidji-Hamburyan, Tarek A El-Ghazawi, and Jason W Triplett. Novel models of visual topographic map alignment in the superior colliculus. *PLoS Comput. Biol.*, 12(12):e1005315, December 2016.
- [24] Dmitry N Tsigankov and Alexei A Koulakov. A unifying model for activity-dependent and activity-independent mechanisms predicts complete structure of topographic maps in ephrin-a deficient mice. *J. Comput. Neurosci.*, 21(1):101–114, August 2006.
- [25] Daniel Lyngholm, David C Sterratt, J J Johannes Hjorth, David J Willshaw, Stephen J Eglén, and Ian D Thompson. Measuring and modelling the emergence of order in the mouse retinocollicular projection. *bioRxiv*, page 713628, July 2019.
- [26] D J Willshaw and C von der Malsburg. How patterned neural connections can be set up by self-organization. *Proc. R. Soc. Lond. B Biol. Sci.*, 194(1117):431–445, November 1976.
- [27] Teuvo Kohonen. Self-organized formation of topologically correct feature maps. *Biol. Cybern.*, 43(1):59–69, January 1982.
- [28] Keith B Godfrey, Stephen J Eglén, and Nicholas V Swindale. A multi-component model of the developing retinocollicular pathway incorporating axonal and synaptic growth. *PLoS Comput. Biol.*, 5(12):e1000600, December 2009.
- [29] P A Robinson. Neural field theory of synaptic plasticity. *J. Theor. Biol.*, 285(1):156–163, September 2011.
- [30] L F Abbott and S B Nelson. Synaptic plasticity: taming the beast. *Nat. Neurosci.*, 3 Suppl:1178–1183, November 2000.
- [31] Peter Beim Graben and Axel Hutt. Attractor and saddle node dynamics in heterogeneous neural fields. *EPJ Nonlinear Biomedical Physics*, 2(1):4, May 2014.
- [32] Cordula Schwappach, Axel Hutt, and Peter Beim Graben. Metastable dynamics in heterogeneous neural fields. *Front. Syst. Neurosci.*, 9:97, June 2015.
- [33] M Meister, R O Wong, D A Baylor, and C J Shatz. Synchronous bursts of action potentials in ganglion cells of the developing mammalian retina. *Science*, 252(5008):939–943, May 1991.
- [34] Robert C Froemke and Yang Dan. Spike-timing-dependent synaptic modification induced by natural spike trains. *Nature*, 416(6879):433–438, March 2002.
- [35] L I Zhang, H W Tao, and M Poo. Visual input induces long-term potentiation of developing retinotectal synapses. *Nat. Neurosci.*, 3(7):708–715, July 2000.
- [36] Cara B Allen, Tansu Celikel, and Daniel E Feldman. Long-term depression induced by sensory deprivation during cortical map plasticity in vivo. *Nat. Neurosci.*, 6(3):291–299, February 2003.
- [37] H Markram, J Lübke, M Frotscher, and B Sakmann. Regulation of synaptic efficacy by coincidence of postsynaptic APs and EPSPs. *Science*, 275(5297):213–215, January 1997.
- [38] Ami Citri and Robert C Malenka. Synaptic plasticity: multiple forms, functions, and mechanisms. *Neuropsychopharmacology*, 33(1):18–41, January 2008.
- [39] James Joseph Wright and Paul David Bourke. On the dynamics of cortical development: synchrony and synaptic self-organization. *Front. Comput. Neurosci.*, 7:4, February 2013.
- [40] S Coombes. Waves, bumps, and patterns in neural field theories. *Biol. Cybern.*, 93(2):91–108, August 2005.
- [41] James B Ackman, Timothy J Burbridge, and Michael C Crair. Retinal waves coordinate patterned activity throughout the developing visual system. *Nature*, 490(7419):219–225, October 2012.

- [42] Joseph Sirosh and Risto Miikkulainen. Cooperative self-organization of afferent and lateral connections in cortical maps. *Biol. Cybern.*, 71(1):65–78, May 1994.
- [43] Penphimon Phongphanphanee, Robert A Marino, Katsuyuki Kaneda, Yuchio Yanagawa, Douglas P Munoz, and Tadashi Isa. Distinct local circuit properties of the superficial and intermediate layers of the rodent superior colliculus. *Eur. J. Neurosci.*, 40(2):2329–2343, July 2014.
- [44] P A Robinson, C J Rennie, D L Rowe, S C O’Connor, and E Gordon. Multiscale brain modelling. *Philos. Trans. R. Soc. Lond. B Biol. Sci.*, 360(1457):1043–1050, May 2005.
- [45] Xuefeng Shi, Yanjiao Jin, and Jianhua Cang. Transformation of feature selectivity from membrane potential to spikes in the mouse superior colliculus. *Front. Cell. Neurosci.*, 12:163, June 2018.
- [46] Onkar S Dhande, Ethan W Hua, Emily Guh, Jonathan Yeh, Shivani Bhatt, Yueyi Zhang, Edward S Ruthazer, Marla B Feller, and Michael C Crair. Development of single retinofugal axon arbors in normal and $\beta 2$ Knock-Out mice. *J. Neurosci.*, 31(9):3384–3399, March 2011.
- [47] J. Burkart. Mathematica markov chain monte carlo. <https://github.com/joshburkart/mathematica-mcmc>, 2017.
- [48] Andrew Gelman and Donald B Rubin. Inference from iterative simulation using multiple sequences. *SSO Schweiz. Monatsschr. Zahnheilkd.*, 7(4):457–472, November 1992.
- [49] A Takeuchi and S Amari. Formation of topographic maps and columnar microstructures in nerve fields. *Biol. Cybern.*, 35(2):63–72, November 1979.
- [50] Hong-Ping Xu, Timothy J Burbridge, Ming-Gang Chen, Xinxin Ge, Yueyi Zhang, Zhimin Jimmy Zhou, and Michael C Crair. Spatial pattern of spontaneous retinal waves instructs retinotopic map refinement more than activity frequency. *Dev. Neurobiol.*, 75(6):621–640, June 2015.
- [51] Jay Demas, Stephen J Eglén, and Rachel O L Wong. Developmental loss of synchronous spontaneous activity in the mouse retina is independent of visual experience. *J. Neurosci.*, 23(7):2851–2860, April 2003.
- [52] Keith B Godfrey and Stephen J Eglén. Theoretical models of spontaneous activity generation and propagation in the developing retina. *Mol. Biosyst.*, 5(12):1527–1535, December 2009.

Appendix: A

Lemma 1. The synaptic change $\frac{dS_p}{dT}$ induced by a given input stimulus A_p which terminates at some arbitrary t_1 can be well approximated by a similar input stimulus A that terminates at $t = \infty$ i.e. $|\frac{dS_p}{dT} - \frac{dS}{dT}| < \epsilon$ for $\epsilon \ll 1$.

Proof. Consider a function $A(y, t)$ which propagates to infinity and induces an activity in the post-synaptic field of $U(x, t)$. For physical reasons this function must decay rapidly at infinity implying for all real t_j :

$$\int_{t_j}^{\infty} A(y, t) dt = \epsilon_j. \quad (31)$$

Then, due to the rapid decay of the of plasticity function we also have that for all physical realisations of u and for all t :

$$\int_{-\infty}^{\infty} H(\tau) U_i(t + \tau) d\tau = \xi_i < \infty. \quad (32)$$

Then, consider the functions $A(y, t) = \Theta(t)h(y, t)$ and $A_p(y, t) = (\Theta(t) - \Theta(t - t_1))h(y, t)$, and the functions $U(x, t)$ and $U_p(x, t)$ which are induced activities from stimulus A and A_p . Observe that as a result of the rapidly decaying plasticity window there exists some ξ such that:

$$\left| \int_{t_1}^{\infty} H(\tau) (U_p(x, t) - U(x, t)) d\tau \right| < \xi, \quad (33)$$

and:

$$\left| \int_{-\infty}^0 H(\tau) (u_p(x, t) - u(x, t)) d\tau \right| < \xi, \quad (34)$$

for all x and t . Also, observe that in the limit $t_1 \rightarrow \infty$, ξ tends to zero. Now let $\epsilon_2 = \xi \int_0^{t_1} A(y, t)$ and note that in the limit $t_1 \rightarrow \infty$ this ϵ_2 will also tend to zero, as the integral of $A(y, t)$ is bounded. Finally, suppose $\int_{t_1}^{\infty} A(y, t) dt < \epsilon_1$. Then, $\epsilon = K_0(\xi\epsilon_1 + 2\epsilon_2)$ may be made arbitrarily small for sufficiently large t_1 . Now consider the synaptic change induced by the truncated function A_p :

$$\frac{dS_p(x, y, T)}{dT} = K_0 \int_{-\infty}^{\infty} A_p(y, t) \int_{-\infty}^{\infty} H(\tau) U_p(x, t + \tau) d\tau dt \quad (35)$$

$$< K_0 \int_0^{t_1} h(y, t) \left(\int_{-\infty}^{\infty} H(\tau) U(x, t + \tau) d\tau + 2\xi \right) dt \quad (36)$$

$$< K_0 \int_{-\infty}^{\infty} \Theta(t) h(y, t) \int_{-\infty}^{\infty} H(\tau) U(x, t + \tau) d\tau dt + \quad (37)$$

$$< \frac{dS(x, y, T)}{dT} + \epsilon. \quad (38)$$

Therefore, it is a sufficiently good approximation to consider the stimulus propagating to infinity, rather than the stimulus truncated at time $t = t_1$ when calculating the synaptic change. \square